nature climate change

LETTERS

PUBLISHED ONLINE: 26 JANUARY 2015 | DOI: 10.1038/NCLIMATE2492

Increased frequency of extreme La Niña events under greenhouse warming

Wenju Cai[1,2]*, Guojian Wang[1,2], Agus Santoso[3], Michael J. McPhaden[4], Lixin Wu[2], Fei-Fei Jin[5], Axel Timmermann[6], Mat Collins[7], Gabriel Vecchi[8], Matthieu Lengaigne[9], Matthew H. England[3], Dietmar Dommenget[10], Ken Takahashi[11] and Eric Guilyardi[9,12]

The El Niño/Southern Oscillation is Earth's most prominent source of interannual climate variability, alternating irregularly between El Niño and La Niña, and resulting in global disruption of weather patterns, ecosystems, fisheries and agriculture[1–5]. The 1998–1999 extreme La Niña event that followed the 1997–1998 extreme El Niño event[6] switched extreme El Niño-induced severe droughts to devastating floods in western Pacific countries, and vice versa in the southwestern United States[4,7]. During extreme La Niña events, cold sea surface conditions develop in the central Pacific[8,9], creating an enhanced temperature gradient from the Maritime continent to the central Pacific. Recent studies have revealed robust changes in El Niño characteristics in response to simulated future greenhouse warming[10–12], but how La Niña will change remains unclear. Here we present climate modelling evidence, from simulations conducted for the Coupled Model Intercomparison Project phase 5 (ref. 13), for a near doubling in the frequency of future extreme La Niña events, from one in every 23 years to one in every 13 years. This occurs because projected faster mean warming of the Maritime continent than the central Pacific, enhanced upper ocean vertical temperature gradients, and increased frequency of extreme El Niño events are conducive to development of the extreme La Niña events. Approximately 75% of the increase occurs in years following extreme El Niño events, thus projecting more frequent swings between opposite extremes from one year to the next.

During typical La Niña events, the central-to-eastern equatorial Pacific is colder than normal, inhibiting formation of rain-producing clouds there, but enhancing atmospheric convection and rainfall in the western equatorial Pacific. The associated atmospheric circulation generates extreme weather events in many parts of the world, including droughts in the southwestern United States[1,14] and eastern equatorial Pacific regions, floods in the western Pacific and central American countries[1,15], and increased land-falling west Pacific cyclones and Atlantic hurricanes[2,16,17].

La Niña-related sea surface temperate (SST) anomaly patterns, however, differ from event to event (Fig. 1a,b). Compared with the weak event of 1995, cold anomalies of the 1998 extreme event peaked notably farther west, and exerted much greater impacts. During 1998, extreme events occurred, in part linked to the developing 1998–1999 La Niña event. The southwestern United States experienced one of the most severe droughts in history[4,7,18]. Venezuela endured flash flooding and landslides that killed 25,000 to 50,000 people[19]. In China, river floods and storms led to the death of thousands, and displaced over 200 million people[20]. Bangladesh experienced one of the most destructive flooding events in modern history, with over 50% of the country's land area flooded, leading to severe food shortages and the spread of waterborne epidemic diseases, killing several thousand people and affecting over 30 million more[21–23]. The 1998 North Atlantic hurricane season saw one of the deadliest and strongest hurricanes (Mitch) in the historical record[4], claiming more than 11,000 lives in Honduras and Nicaragua[24].

The 1998–1999 La Niña event occurred after the 1997–1998 extreme El Niño event—referred to as the climate event of the twentieth century[3], inducing swings of opposite extremes from one year to the next. Recent studies have shown a greenhouse warming-induced increase in extreme El Niño events[10], eastward-propagating El Niño[12], and El Niño-related equatorward swings of the South Pacific convergence zone[25]. However, the future characteristics of La Niña events are yet to be examined. Here we show that greenhouse warming leads to a significant increase in the frequency of extreme La Niña events.

Extreme La Niña events feature the coldest sea surface anomalies in the central Pacific, a pattern not a mirror image of extreme El Niño events, which have maximum warm anomalies in the eastern equatorial Pacific[8–10]. Thus, the non-symmetric dynamics of these two climate extremes needs to be studied separately using at least two indices[8]. To capture the essential feature of an extreme La Niña, we apply empirical orthogonal function (EOF) analysis to deconvolve the spatio-temporal SST variability into orthogonal modes, each described by a principal spatial pattern and an associated principal component (PC) time series (see Methods). We focus on satellite-era observations (Methods), and austral summer/boreal winter (December–February), when typical La Niña events peak.

In the positive phase, EOF1 (Fig. 1c) shows a canonical La Niña pattern, and EOF2 exhibits a cooling in the central Pacific and a warming in both the eastern and western part of the basin (Fig. 1d),

[1]CSIRO Oceans and Atmosphere Flagship, Aspendale, Victoria 3195, Australia. [2]Physical Oceanography Laboratory, Qingdao Collaborative Innovation Center of Marine Science and Technology, Ocean University of China, Qingdao 266003, China. [3]Australian Research Council (ARC) Centre of Excellence for Climate System Science, Level 4 Mathews Building, The University of New South Wales, Sydney 2052, Australia. [4]NOAA/Pacific Marine Environmental Laboratory, Seattle, Washington 98115, USA. [5]Department of Meteorology, SOEST, University of Hawaii, Honolulu, Hawaii 96822, USA. [6]IPRC, Department of Oceanography, SOEST, University of Hawaii, Honolulu, Hawaii 96822, USA. [7]College of Engineering Mathematics and Physical Sciences, Harrison Building, Streatham Campus, University of Exeter, Exeter EX1 3PB, UK. [8]Geophysical Fluid Dynamics Laboratory/NOAA, Princeton, New Jersey 08540-6649, USA. [9]Laboratoire d'Océanographie et du Climat: Expérimentation et Approches Numériques (LOCEAN), IRD/UPMC/CNRS/MNHN, Paris Cedex 05, France. [10]School of Mathematical Sciences, Monash University, Clayton, Victoria 3800, Australia. [11]Instituto Geofísico del Perú, Lima 169, Perú. [12]NCAS-Climate, University of Reading, Reading RG6 6BB, UK. *e-mail: wenju.cai@csiro.au

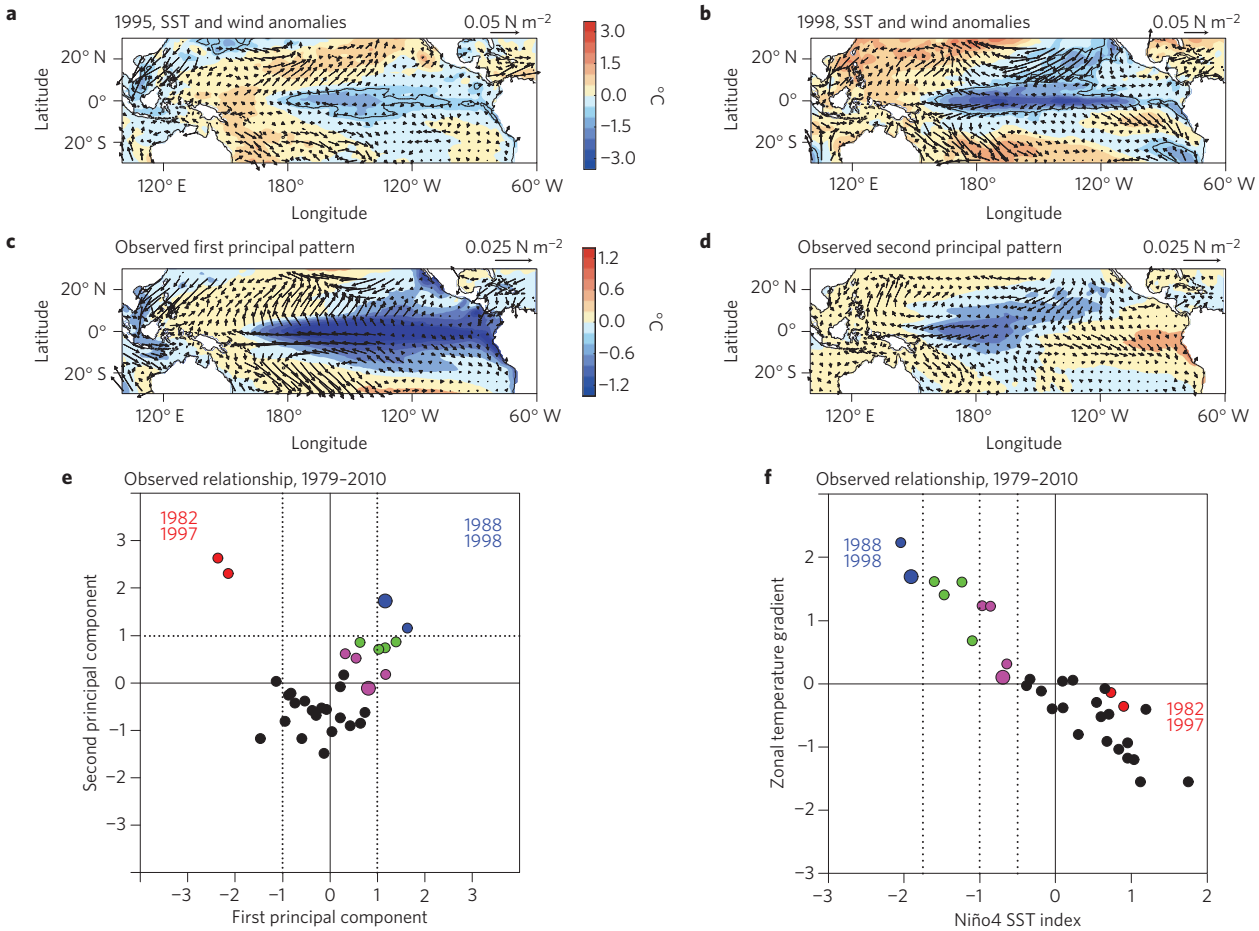

Figure 1 | Identification of observed extreme La Niña events. a,**b**, December–February average SST anomalies (shading, −0.75 °C contour highlighted by a black curve) and surface wind stress anomalies (vectors, scale shown in the top right corner of each panel) associated with a weak (**a**) and extreme (**b**) La Niña. **c**,**d**, Principal variability patterns of SST obtained by applying EOF analysis to satellite-era SST anomalies (see Methods), in the equatorial region (15° S–15° N, 140° E–280° E). The SST anomalies and wind stress vectors are presented as linear regression onto the EOF time series. **e**, Relationship between the two principal component time series. An extreme La Niña event (blue dots, big blue 1998) can be defined as when the first and second principal component are both greater than 1.0 standard deviation (s.d.). Extreme El Niño events are indicated by red dots. Green dots indicate moderate La Niña, and purple dots weak La Niña (big purple 1995), defined as when quadratically detrended Niño4 is greater than 0.5 s.d. but less than 1.0 s.d. in amplitude. Black dots indicate all other years. **f**, Relationship between Niño4 and a time series of the Maritime continent region (5° S–5° N, 100° E–125° E)–central Pacific (Niño4, 5° S–5° N, 160° E–150° W) surface temperature gradient, with a correlation coefficient of $r = -0.93$. Colours are the same as in **e**.

resembling a La Niña Modoki pattern[26]. The two associated time series exhibit a V-shaped nonlinear relationship (Fig. 1e). The 1982–1983 and 1997–1998 extreme El Niño events manifest as a superimposition of a strong canonical El Niño pattern (EOF1, sign reversed), and an EOF2 pattern with a cooling offsetting warming over the central Pacific in EOF1 (big red dots, Fig. 1e), leading to the warmest SST confined in the eastern equatorial Pacific[10].

The 1998 extreme La Niña is described by the sum of a positive EOF1 and a positive EOF2 (big blue dot, Fig. 1e and Supplementary Fig. 1), and is characterized by maximum cold anomalies near the Niño4 region (5° S–5° N, 160° E–150° W; Fig. 1b). In contrast, with EOF2 close to zero, the 1995 weak La Niña (big purple dot, Fig. 1e) can be largely described by a positive EOF1 (Supplementary Fig. 1), with weaker anomalous cooling (for example, the −0.75 °C contour) located east of the Date Line (Fig. 1a,b). The stronger the magnitude of EOF2, the colder the SST anomalies in the Niño4 region (Supplementary Fig. 2a). The sum of the two EOFs, or more precisely the value of $(PC1 + PC2)\sqrt{2}$ (ref. 8), essentially measures the strength of La Niña, and is almost identical to Niño4 ($r = -0.96$; Supplementary Fig. 2b) except the two extreme El Niño events. As such, we simply use the Niño4 index. Defining an extreme La Niña as when the amplitude of Niño4 is greater than the 1.75 standard deviation (s.d.) value captures the extreme La Niña events of 1988–1989 and 1998–1999. Lowering the threshold to 1.5 s.d. includes also the 1999–2000 event.

Another implication of EOF2 (Fig. 1d) is that the west-minus-east SST gradient between the Maritime continent (5° S–5° N, 100° E–125° E) and the Niño4 region is stronger during an extreme La Niña event compared with during weak La Niña events (Fig. 1a,b). This gradient, taken directly from surface air temperatures, is highly correlated with the Niño4 index ($r = -0.95$; Fig. 1f). That is, the colder the Niño4 region, the stronger this gradient.

The 1998–1999 extreme La Niña peaked several months after the heat discharge associated with the 1997–1998 extreme El Niño[27,28] reached its maximum. Similarly, the 1988–1989 extreme La Niña occurred after the discharge by the consecutive 1986–1987 and 1987–1988 El Niño events. In both cases, as the thermocline across the equatorial Pacific shoaled, upwelling initiated the onset of unusually cold SSTs in the central basin. This cooling strengthened the easterly winds, which piled up warm water in the western Pacific, gradually increasing the Maritime region–central Pacific

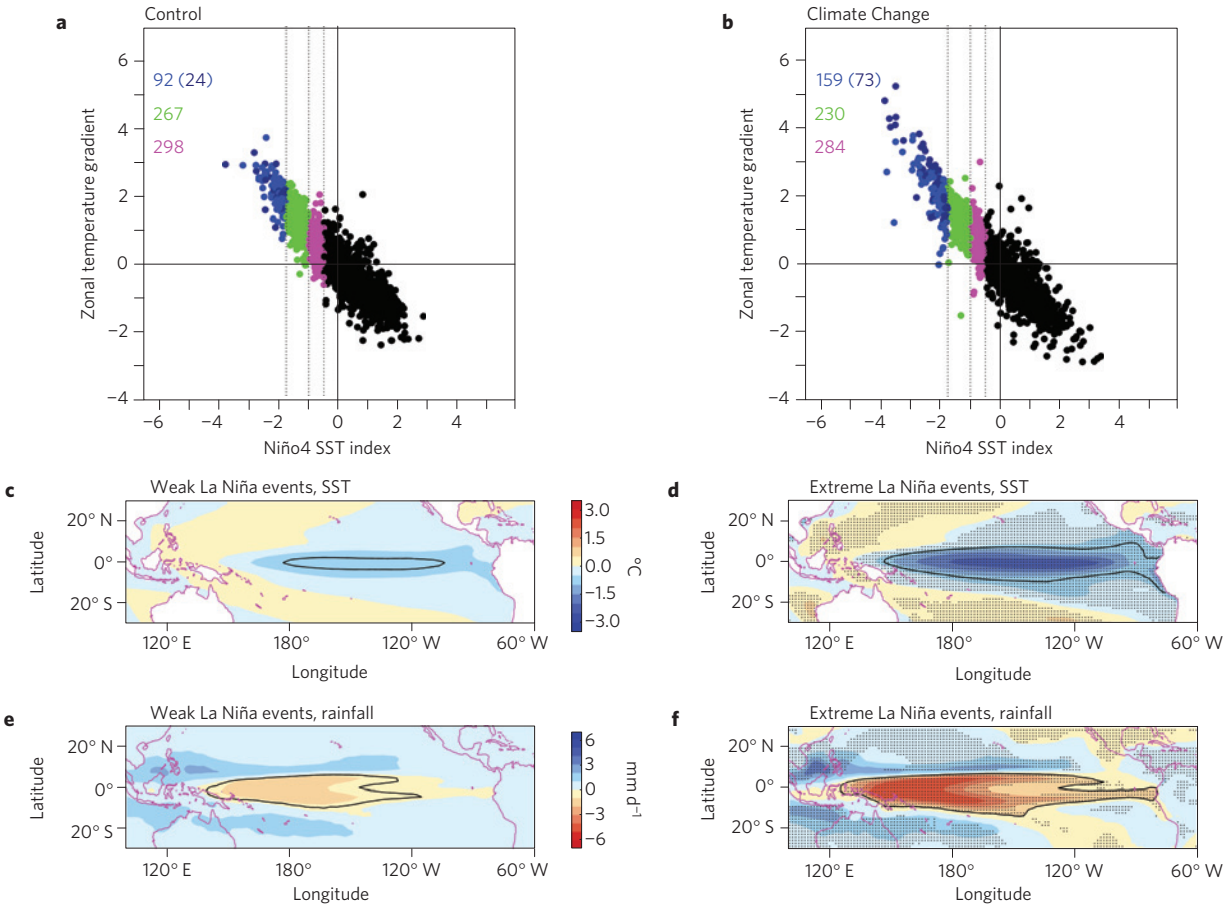

Figure 2 | Identification of model extreme La Niña events using 21 selected models. An extreme La Niña is defined as Niño4 amplitude greater than 1.75 s.d. **a**,**b**, Relationship of Niño4 with surface temperature gradients between the Maritime continent region (5° S–5° N, 100° E–125° E) and the central Pacific (5° S–5° N, 160° E–150° W), for the Control (**a**) and Climate Change (**b**) period. Blue, green and purple dots indicate extreme (with |Niño4| > 1.75 s.d.), moderate (1.0 s.d. < |Niño4| < 1.75 s.d.) and weak (0.5 s.d. < |Niño4| < 1.0 s.d.) La Niña. Black dots are all the years that don't fall into these criteria. The number of different types of La Niña event is indicated, with dark blue dots and the dark blue number in brackets indicating extreme La Niña events that follow an extreme El Niño, defined as in ref. 10. **c**,**d**, December–February composite SST anomalies (shading, colour scale applies to both panels) for weak and extreme La Niña events. **e**,**f**, The same as in **c**,**d**, respectively, but for rainfall anomalies (colour scale applies to both panels). Areas with stipples in **d**,**f** indicate differences between extreme and weak La Niña events that are statistically significant above the 95% confidence level. The −0.75 °C SST contour in **c**,**d**, and the −1.0 mm d^{-1} precipitation contour in **e**,**f** are indicated by a black curve.

temperature gradient. This in turn drove further anomalous upwelling, shallowing of the thermocline, and westward and poleward surface currents in the Niño4 region, through the Bjerknes positive feedback, in which the stronger easterly winds and resultant westward-flowing currents, poleward flows, and upwelling reinforce the initial cooling. A heat budget analysis shows that processes involving these anomalies in the pre-peak months (August–December) are dominant in driving the Niño4 cold anomalies (Supplementary Text). These are zonal advection (especially the anomalous westward advection of anomalous zonal SST gradient, or nonlinear zonal advection; Supplementary Fig. 3c), meridional advection (Supplementary Fig. 3h) and Ekman pumping (anomalous upward advection of mean vertical temperature gradient; Supplementary Fig. 3k)—all leading to cooling in the Niño4 region. Each of these cooling processes involves anomalous easterly winds over the central-to-west Pacific, which are in turn tightly linked to the Maritime–central Pacific surface temperature gradient (Supplementary Fig. 4).

We selected 21 (out of 32) Coupled Model Intercomparison Project phase 5 (CMIP5) models able to simulate nonlinear processes associated with extreme El Niño/Southern Oscillation events[10] (see Methods). These models were forced with historical anthropogenic and natural forcings, and future greenhouse gas emission scenarios, covering 1900–2099. We defined an extreme La Niña event using quadratically detrended Niño4 anomalies, and compared the frequency in the first (1900–1999) and second (2000–2099) 100-year periods, referred to as the Control and Climate Change periods, respectively.

Using a threshold value of 1.75 s.d. yields a 73% increase in the frequency of extreme La Niña events, from one event every 23 years to one every 13 years. The robustness of this result is underpinned by a strong inter-model consensus, with only 4 out of 21 models producing a reduction (Supplementary Table 1), statistically significant according to a bootstrap test (Methods). The differences in SST and rainfall anomaly patterns between model extreme and weak La Niña events are also significant in the Niño4 region (Fig. 2c,d). Furthermore, approximately 75% of the increased extreme La Niña events occur in the year following an extreme El Niño event, as defined in ref. 10. Raising the threshold value to 2.0 s.d. produces a near doubling in frequency with only three models showing a decrease, further supporting our result (Supplementary Table 1). Examination of impact from a possible change in seasonal cycle, inclusion of Niño4 SST skewness in the model selection, formation of anomalies, detrending procedure in SST, and using all models, confirms the robustness of these results (Supplementary Tables 2–6 and Text). In particular, even when all models are used, there is still a

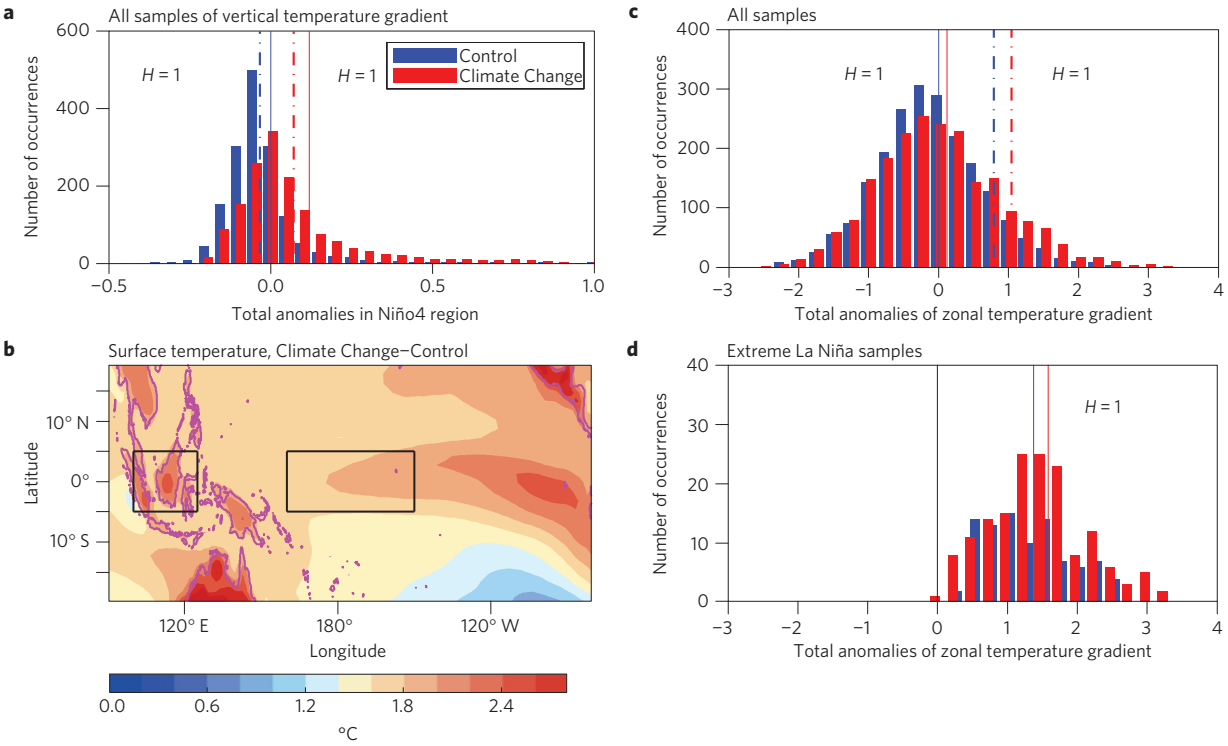

Figure 3 | Multi-model statistics in August–December associated with the increase in frequency of extreme La Niña events. a, Multi-model ensemble histogram of the upper ocean vertical temperature gradient in the Niño4 region, defined as the average of temperature in the top 50 m minus temperature at 60 m, showing an increase in the gradient for all samples. Values are separated into 0.05 bins centred at the tick point for the Control (blue) and Climate Change (red) periods. The multi-model medians for the Control (solid blue line) and the Climate Change (solid red line) periods are indicated. The corresponding values for all La Niña samples alone (Niño4 < -0.5 s.d.) are also indicated by dashed blue (Control) and dashed red (Climate Change) lines. **b**, Multi-model ensemble average of surface temperature changes (in °C) between the average over the Climate Change and the Control periods; only values significant above the 95% confidence level are plotted. The rectangles indicate areas for constructing zonal SST gradient. **c**,**d**, Multi-model ensemble histogram of the Maritime–central Pacific surface temperature gradient (referenced to the mean of the Control period) for all samples and for extreme La Niña samples alone, respectively. Values are separated into 0.25 bins centred at the tick point for the Control (blue) and Climate Change (red) periods. As in **a**, the multi-model medians for the Control (blue line) and the Climate Change (red line) periods are also indicated. The shift histograms in **a**,**c** and **d** are statistically significant above the 95% confidence level (as indicated by $H=1$) according to a two-sided Student t-test.

strong inter-model consensus. Further, in a set of perturbed physics ensemble experiments, in which the well-known cold SST bias is removed, the increase in the frequency is even greater (Supplementary Table 7), indicating that our result holds without the bias. Again, most of the increase occurs after an extreme El Niño event.

Our result may seem counterintuitive, because the Walker Circulation, which is enhanced during La Niña, is projected to weaken[29]. Although the weakened Walker Circulation underlies the projected increase in extreme El Niño frequency[10], the mechanism for extreme La Niña frequency increase is not the opposite of that for extreme El Niño. In fact, it is linked because the increased frequency of extreme El Niño events leads to more occurrences of a discharged state that favours development of an extreme La Niña, as occurred in 1998–1999.

In addition, feedback processes responsible for extreme La Niña are more efficient in the Climate Change period. As the thermocline shoals and greenhouse gas forcing continues to warm the ocean from the surface, the vertical temperature gradient increases during the Climate Change period (Fig. 3a). This is conducive to an enhanced efficiency of the Ekman pumping term, an important process for extreme La Niña events as supported by the inter-model relationship between the increase in the frequency and change in the vertical temperature gradient (Supplementary Fig. 5). Further, under enhanced greenhouse conditions, the Maritime continent region warms faster than the central equatorial Pacific (Fig. 3b). Suppressed convection in the Niño4 region is a key feature during extreme La Niña (Supplementary Fig. 6). The faster Maritime warming means that a smaller SST cooling is sufficient to suppress convection in the Niño4 region to beyond a threshold (Supplementary Fig. 7), as the convection centre is easier to move to the Maritime region. This makes it easier to trigger Bjerknes feedback, involving positive zonal SST gradients and easterly winds (Supplementary Fig. 8), hence westward zonal currents and nonlinear zonal advection, important for the growth of the Niño4 SST cool anomalies. In association, there are more frequent occurrences of positive zonal temperature gradients surpassing a threshold (Fig. 3c,d). These processes (summarized in Supplementary Fig. 9) occur despite a weakening Walker circulation[29], which at other times favours strong negative gradients, of which the frequency also increases (Fig. 3c).

Consistent with the increased frequency in extreme La Niña events, there are more occurrences of extreme low rainfall over the Niño4 region in the Climate Change period than in the Control period (Fig. 4). Overall, in the Niño4 region, there are more extreme cold SST and low rainfall anomalies. Despite this, differences between the two periods in the detrended rainfall teleconnection pattern of extreme La Niña events are not significant in most regions (left column, Supplementary Fig. 10). Thus, in general the impacts of extreme La Niña events experienced in the Control period will repeat more frequently in the Climate Change period. However, in terms of total rainfall anomalies referenced to the Control period, in some South Pacific Island countries, such as the Solomon Islands, where extreme La Niña events cause floods, the impact is more

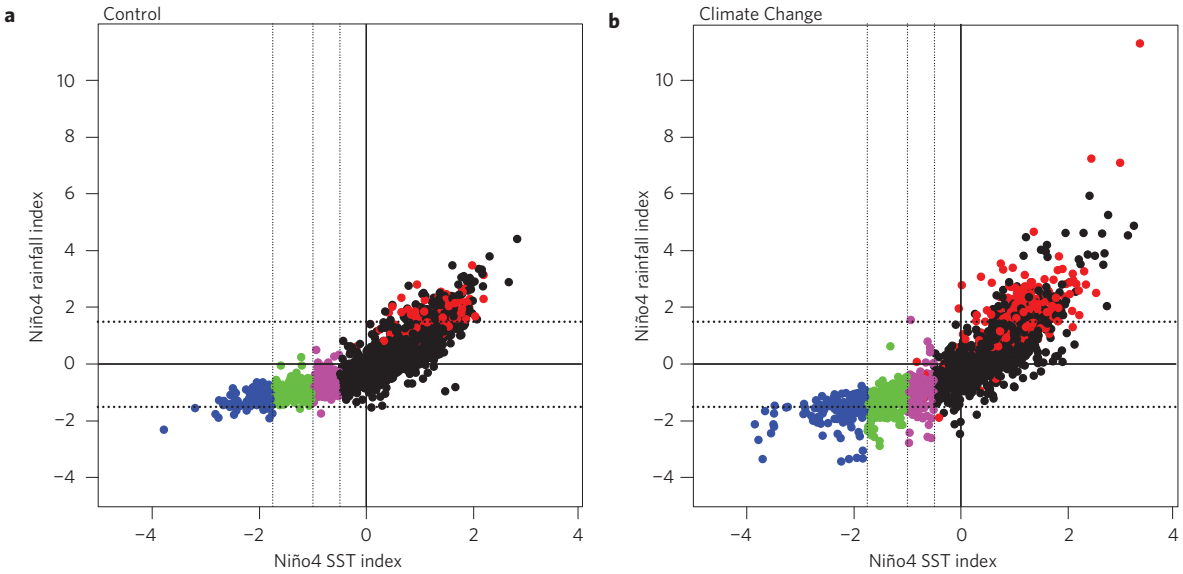

Figure 4 | Relationship between detrended Niño4 rainfall and Niño4 SST. a,**b**, For the Control (**a**) and Climate Change (**b**) periods. Blue, green and purple dots indicate extreme (|Niño4| > 1.75 s.d.), moderate (1 s.d. < |Niño4| < 1.75 s.d.) and weak (0.5 s.d. < |Niño4| < 1.0 s.d.) La Niña events, with a negative Niño4. Red dots indicate extreme El Niño events as identified by ref. 10, and black dots indicate all other years.

severe in the Climate Change than Control period (right column, Supplementary Fig. 10). The intensified impact as seen in the detrended Niño4 rainfall anomalies is consistent with a nonlinear rainfall sensitivity to SST arising from warmer background temperatures in the Climate Change period[30].

Our result of a greenhouse-induced increase in occurrences of extreme La Niña events is consistent with an increased frequency of extreme El Niño that provides a favourable condition for extreme La Niña. This occurs amid a faster warming over the Maritime continent region than the central equatorial Pacific and increasing vertical temperature gradients that are conducive to extreme La Niña events. We note that the weakening Walker circulation that underlies the projected increase in extreme El Niño frequency is still a matter of debate and model biases in El Niño/Southern Oscillation simulation can introduce uncertainties. Nevertheless, the overall increased frequency in extreme La Niña events, most of which occur in the year after an extreme El Niño, has important implications. It means more occurrences of devastating weather events, and more frequent swings of opposite extremes from one year to the next, with profound socio-economic consequences.

Methods

EOF analysis and characterization of extreme La Niña events. EOF analysis was applied to observed SST anomalies, referenced to the long-term mean since 1979, in an equatorial domain (15° S–15° N, 140° E–80° W). The extreme La Niña events were diagnosed using a suite of distinct process-based indicators associated with the two EOFs, such as low temperature, low rainfall and wind anomalies. In particular, the SST anomalies are centred at the central Pacific during extreme La Niña, as opposed to the eastern equatorial Pacific during extreme El Niño. The difference in spatial patterns is captured by a different combination of two principal variability patterns. EOF1 reflects a canonical La Niña pattern embedded in the commonly used Niño3 index, featuring cool and dry anomalies extending from the eastern equatorial Pacific to the central Pacific. EOF2 resembles the La Niña Modoki pattern[26], featuring cool and dry anomalies in the central Pacific, but warm and wet anomalies in the far western equatorial Pacific. Thus, an extreme La Niña is an appropriately weighted superposition of the two patterns, giving rise to an anomaly centred in the central Pacific. As such, a depiction of extreme La Niña must use a different index from that for extreme El Niño, and we show that an average of SST anomalies over the Niño4 region is an appropriate index.

Model selection and analysis. We used 21 CMIP5 coupled global climate models (CGCMs; Supplementary Table 1) forced with historical anthropogenic and natural forcings, and future greenhouse gases under the Representative Concentration Pathway 8.5 (ref. 13) emission scenario, covering a 200-year period. These were chosen from a total of 32 models, on the basis of their ability to simulate extreme La Niña events (Supplementary Table 1). As extreme La Niña tends to occur after extreme El Niño, we select models that are also able to simulate extreme El Niño. These were selected in terms of two features[10]: the positive skewness of rainfall anomalies, and the ability to generate rainfall greater than 5 mm d^{-1} over the eastern equatorial Pacific. Only a subgroup of CGCMs simulate the observed nonlinear ocean–atmosphere coupling that characterizes extreme El Niño, as depicted by the positive skewness of rainfall anomalies over the eastern equatorial Pacific during austral summer (December–February), which is 2.7 in observations since 1979. The level of nonlinearity varies vastly among CGCMs, and we considered positive skewness of 1 as our threshold. Out of the 32 CGCMs, 21 models satisfy the rainfall skewness criterion. The selected CGCMs yield a mean skewness of 2.6, close to the observed value of 2.7 (Supplementary Table 1).

All 21 selected CGCMs reproduce the observed extreme La Niña pattern. Before the analysis, data were interpolated onto a common grid of 1.5° latitude by 1.5° longitude. As for the observations, EOF analysis was carried out for each individual model using SST anomalies referenced to the mean over the Control period. All 21 models produce the nonlinear relationship between the two leading EOFs, indicating their ability to generate the nonlinear equatorial positive feedback associated with extreme La Niña events. On the basis of analysis of observed SSTs, we used a quadratically detrended Niño4 index over the full 200-year period to describe La Niña events. Applying quadratical detrending over each of the periods separately yields almost identical results.

We tested the sensitivity of our results to varying threshold values for Niño4 (Supplementary Table 1). We also tested our results using a negative Niño4 SST skewness (Supplementary Text and Table 2), as observations show a negative skewness of −0.44 (using data since 1979). In all cases, including using all available models (Supplementary Text), there is an increase in the occurrences of extreme La Niña events from the Control to the Climate Change period, with a strong inter-model consensus.

Statistical significance test. We used a bootstrap method to examine whether the increased frequency is statistically significant. The 2,100 samples from the 21 models in the Control period were re-sampled randomly to construct 10,000 realizations of 2,100-year records. In the random re-sampling process, any extreme La Niña event is allowed to be selected again. The standard deviation of the extreme La Niña frequency using a threshold value of Niño4 amplitude greater than 1.75 s.d. in the inter-realization is 9.4 events per 2,100 years, far smaller than the difference of 67 events per 2,100 years between the Climate Change and the Control periods. Using a threshold value of Niño4 amplitude greater than 1.5 s.d. in the inter-realization yields 12 events per 2,100 years, also far smaller than the difference of 65 events per 2,100 years between the Climate Change and the Control periods (Fig. 3a,b), indicating strong statistical significance. Using a threshold value of Niño4 amplitude greater than 2.0 s.d.

again shows a strong significance. Increasing the realizations to 20,000 or 30,000 in the bootstrapping methodology yields essentially identical results.

Received 29 July 2014; accepted 2 December 2014; published online 26 January 2015

References

1. Ropelewski, C. F. & Halpert, M. S. Global and regional scale precipitation patterns associated with the El Niño/Southern Oscillation. *Mon. Weath. Rev.* **115,** 1606–1626 (1987).
2. Bove, M. C., O'Brien, J. J., Eisner, J. B., Landsea, C. W. & Niu, X. Effect of El Niño on US landfalling hurricanes, revisited. *Bull. Am. Meteorol. Soc.* **79,** 2477–2482 (1998).
3. Changnon, S. A. Impacts of 1997–98 El Niño generated weather in the United States. *Bull. Am. Meteorol. Soc.* **80,** 1819–1827 (1999).
4. Bell, G. D. *et al.* Climate assessment for 1998. *Bull. Am. Meteorol. Soc.* **80,** 1040–1040 (1999).
5. McPhaden, M. J., Zebiak, S. E. & Glantz, M. H. ENSO as an integrating concept in Earth science. *Science* **314,** 1740–1745 (2006).
6. McPhaden, M. J. El Niño: The child prodigy of 1997–98. *Nature* **398,** 559–562 (1999).
7. Hoerling, M. & Kumar, A. The perfect ocean for drought. *Science* **299,** 691–694 (2003).
8. Takahashi, K., Montecinos, A., Goubanova, K. & Dewitte, B. ENSO regimes: Reinterpreting the canonical and Modoki El Niño. *Geophys. Res. Lett.* **38,** L10704 (2011).
9. Dommenget, D., Bayr, T. & Frauen, C. Analysis of the non-linearity in the pattern and time evolution of El Niño southern oscillation. *Clim. Dynam.* **40,** 2825–2847 (2013).
10. Cai, W. *et al.* Increasing frequency of extreme El Niño events due to greenhouse warming. *Nature Clim. Change* **4,** 111–116 (2014).
11. Power, S., Delage, F., Chung, C., Kociuba, G. & Keay, K. Robust twenty-first-century projections of El Niño and related precipitation variability. *Nature* **502,** 541–545 (2013).
12. Santoso, A. *et al.* Late-twentieth-century emergence of the El Niño propagation asymmetry and future projections. *Nature* **504,** 126–130 (2013).
13. Taylor, K. E., Stouffer, R. J. & Meehl, G. A. An overview of CMIP5 and the experimental design. *Bull. Am. Meteorol. Soc.* **93,** 485–498 (2012).
14. Kiladis, G. N. & Diaz, H. F. Global climate anomalies associated with extremes in the Southern Oscillation. *J. Clim.* **2,** 1069–1090 (1989).
15. Hoyos, N., Escobar, J., Restrepo, J. C., Arango, A. M. & Ortiz, J. C. Impact of the 2010–2011 La Niña phenomenon in Colombia, South America: The human toll of an extreme weather event. *Appl. Geogr.* **39,** 16–25 (2013).
16. Wu, M. C., Chang, W. L. & Leung, W. M. Impact of El Niño-Southern Oscillation events on tropical cyclone landfalling activities in the western North Pacific. *J. Clim.* **17,** 1419–1428 (2004).
17. Gray, W. M. Atlantic seasonal hurricane frequency: Part I: El Niño and 30-mb quasibiennial oscillation influences. *Mon. Weath. Rev.* **112,** 1669–1683 (1984).
18. Cole, J. E., Overpeck, J. T. & Cook, E. R. Multiyear La Niña events and persistent drought in the contiguous United States. *Geophys. Res. Lett.* **29,** http://dx.doi.org/10.1029/2001GL013561 (2002).
19. Takahashi, T., Nakagawa, H., Satofuka, Y. & Kawaike, K. Flood and sediment disasters triggered by 1999 rainfall in Venezuela; a river restoration plan for an alluvial fan. *J. Natural Disast. Sci.* **23,** 65–82 (2001).
20. Jonkman, S. N. Global perspectives on loss of human life caused by floods. *Natural Hazards* **34,** 151–175 (2005).
21. Kunii, O., Nakamura, S., Abdur, R. & Wakai, S. The impact on health and risk factors of the diarrhoea epidemics in the 1998 Bangladesh floods. *Public Health* **116,** 68–74 (2002).
22. Del Ninno, C. & Dorosh, P. A. Averting a food crisis: Private imports and public targeted distribution in Bangladesh after the 1998 flood. *Agric. Econ.* **25,** 337–346 (2001).
23. Mirza, M. M. Q., Warrick, R. A., Ericksen, N. J. & Gavin, G. J. Are floods getting worse in the Ganges, Brahmaputra and Meghna basins? *Environ. Hazards* **3,** 37–48 (2002).
24. Kerle, N., Froger, J. L., Oppenheimer, C. & Van Wyk De Vries, B. Remote sensing of the 1998 mudflow at Casita volcano, Nicaragua. *Int. J. Remote Sensing* **24,** 4791–4816 (2003).
25. Cai, W. *et al.* More extreme swings of the South Pacific Convergence Zone due to greenhouse warming. *Nature* **488,** 365–369 (2012).
26. Ashok, K., Behera, S. K., Rao, S. A., Weng, H. & Yamagata, T. El Niño Modoki and its possible teleconnection. *J. Geophys. Res.* **112,** C11007 (2007).
27. Jin, F. F. An equatorial ocean recharge paradigm for ENSO. Part I: Conceptual model. *J. Atmos. Sci.* **54,** 811–829 (1997).
28. Meinen, C. S. & McPhaden, M. J. Observations of warm water volume changes in the equatorial Pacific and their relationship to El Niño and La Niña. *J. Clim.* **13,** 3551–3559 (2000).
29. Vecchi, G. A. & Soden, B. J. Global warming and the weakening of the tropical circulation. *J. Clim.* **20,** 4316–4340 (2007).
30. Chung, C. T. Y. & Power, S. B. Precipitation response to La Niña and global warming in the Indo-Pacific. *Clim. Dynam.* **43,** 3293–3307 (2014).

Acknowledgements

W.C. and G.W. are supported by the Australian Climate Change Science Program and a CSIRO Office of Chief Executive Science Leader award. A.S. and M.H.E. are supported by the Australian Research Council. D.D. is supported by ARC project 'Beyond the linear dynamics of the El Niño–Southern Oscillation' (DP120101442) and ARC Centre of Excellence for Climate System Science (CE110001028). M.C. was supported by NERC/MoES SAPRISE project (NE/I022841/1). M.J.M. was supported by NOAA, and this is PMEL contribution number 4259.

Author contributions

W.C. conceived the study, directed the analysis, and wrote the initial version of the paper in discussion with G.W. and A.S. G.W. performed the model output analysis. A.S. conducted and wrote the description of the heat budget analysis in the Supplementary Information. All authors contributed to interpreting results, discussion of the associated dynamics, and improvement of this paper.

Additional information

Supplementary information is available in the online version of the paper. Reprints and permissions information is available online at www.nature.com/reprints. Correspondence and requests for materials should be addressed to W.C.

Competing financial interests

The authors declare no competing financial interests.